Comparison of cationic, anionic and neutral hydrogen bonded dimers

Han Myoung Lee,† Anupriya Kumar,† Maciej Kołaski,‡ Dong Young Kim, Eun Cheol Lee, Seung Kyu Min, Mina Park, Young Cheol Choi and Kwang S. Kim*

Received 4th December 2009, Accepted 5th March 2010
First published as an Advance Article on the web 20th April 2010
DOI: 10.1039/b925551f

Short Strong Hydrogen Bonds (SSHBs) play an important role in many fields of physics, chemistry and biology. Since it is known that SSHBs exist in many biological systems, the role of hydrogen bonding motifs has been particularly interesting in enzyme catalysis, bio-metabolism, protein folding and proton transport phenomena. To explore the characteristic features of neutral, anionic and cationic hydrogen bonds, we have carried out theoretical studies of diverse homogeneous and heterogeneous hydrogen bonded dimers including water, peroxides, alcohols, ethers, aldehydes, ketones, carboxylic acids, anhydrides, and nitriles. Geometry optimization and harmonic frequency calculations are performed at the levels of Density Functional Theory (DFT) and Møller–Plesset second order perturbation (MP2) theory. First principles Car–Parrinello molecular dynamics (CPMD) simulations are performed to obtain IR spectra derived from velocity- and dipole-autocorrelation functions. We find that the hydrogen bond energy is roughly inversely proportional to the fourth power of the r(O/N–H) distance. Namely, the polarization of the proton accepting O/N atom by the proton-donating H atom reflects most of the binding energy in these diverse cation/anion/neutral hydrogen bonds. The present study gives deeper insight into the nature of hydrogen-bonded dimers including SSHBs.

1. Introduction

Hydrogen bonds[1] are important in water,[2] solvation,[3] acid–base chemistry,[4] biomolecular systems,[5] molecular recognition,[6] and self-assembly of nanomaterials.[7] Ionic hydrogen bonds play an important role in many physical, chemical and biological phenomena.[8] It is well known that SSHBs exist in various active sites of enzymes and take part in enzyme catalysis.[9] The O–H···O hydrogen bond motifs are important in proton dynamics and transport.[10]

In neutral [–O–H···O–] H-bonded systems, the inter-oxygen distances involved in hydrogen bond formation are ~2.8 Å.[11] Hydrogen bonds such as ═O···H···O═ and –CO–OH···O═CO– are neutral H-bonds exhibiting a resonance phenomenon. In the case of H-bond relays, the inter-oxygen distances become even shorter (down to ~2.64 Å).[12] In anionic $[–O···H···O]^-$ H-bonded systems such as $H_3O_2^-$, the inter-oxygen distance is even shorter (2.5 Å).[13] In various anionic $[–O···H–O–]^-$ organic crystals the inter-oxygen distance is ~2.5 Å (in some cases, r(O···O) is slightly shorter; ~2.46 Å).[14] In cationic $[–O···H^+···O–]$ H-bonded motifs such as $H_5O_2^+$,[15] the r(O···O) distance is only ~2.4 Å.[16]

Homogeneous and heterogeneous dimers comprising ionic H-bonded organic functional groups significantly affect the physical properties of supramolecular networks, acting as hydrogen bond donors or acceptors.[17] The hydrogen bond strength between various components depends on the relative acidity and basicity of monomers. Despite thermochemical studies,[18] it is hard to differentiate between the structures of heterogeneous ionic hydrogen-bonded dimers with a large difference in polarity. The O···HO infrared spectrum (IR) analysis could be useful to observe the effect of different substituents in cationic/anionic and neutral H-bonded systems.

The vibrational modes of hydrogen bonds are characterized by a broad IR spectrum ranging from 800 cm^{-1} for wagging to 3500 cm^{-1} for stretching.[19] A DFT based study suggests that IR frequencies of O···H–O motifs range from 400 cm^{-1} to 2800 cm^{-1}. The red-shift to 2800 cm^{-1} is due to change from the covalent bond to the hydrogen bond.[20] As the distance between the two negatively charged oxygen atoms holding a proton decreases, the hydrogen bond strength increases. In the case of cationic systems, the r(O···O) distance is around 2.4 Å, while the corresponding O–H distance is close to 1.2 Å, which is reflected in the formation of symmetric SSHBs. These SSHBs are found in certain proteins and protonated water clusters.[21] The frequencies associated with the vibrations of the proton involved in SSHB are in the range between 1100 cm^{-1} to 1800 cm^{-1}. These frequencies could be studied with first principles molecular dynamics simulations. However, due to the anharmonic feature of the potential energy with respect to the hydrogen position, the harmonic frequencies can be substantially different from the experimental frequencies. In this situation, the Fourier transform of the velocity-autocorrelation function and dipole-autocorrelation

Center for Superfunctional Materials, Department of Chemistry, Pohang University of Science and Technology, San 31, Hyojadong, Namgu, 790-784 Pohang, South Korea. E-mail: kim@postech.ac.kr
† These authors contributed equally to this work.
‡ Permanent address: Department of Theoretical Chemistry, Institute of Chemistry, University of Silesia, 9 Szkolna Street, 40-006 Katowice, Poland.

function taken from Car–Parrinello molecular dynamics (CPMD) or *ab initio* molecular dynamics simulations can provide a reliable estimation of experimental vibrational frequencies.

In the present work, we examined neutral, anionic and cationic hydrogen bonds in diverse homogeneous and heterogeneous hydrogen-bonded dimers including water, peroxides, alcohols, ethers, aldehydes, ketones, carboxylic acids, anhydrides, and nitriles. The vibrational spectral signatures were assigned to various types of hydrogen bonds. We also studied the influence of the substituent effect on the formation of cationic/anionic and neutral hydrogen bonds. The fingerprints of these hydrogen bonds were identified by spectral analysis of homogeneous and heterogeneous dimers.

2. Calculation methods

We carried out geometry optimization, harmonic frequency analysis, and CPMD simulations of cationic, anionic and neutral homogeneous and heterogeneous dimers. Geometry optimization and harmonic frequency calculations were done at the DFT level with Becke's exchange potential and Lee–Yang–Parr correlation functional (BLYP), Becke's three parameters (B3LYP), and the MP2 level with the aug-cc-pVDZ + diffuse(2s,2p) basis sets (abbreviated as aVDZ++) by using the Gaussian 03 suite of programs.[22] Calculated proton affinities (PAs) of various organic molecules comprising different functional groups are in good agreement with the experimental values (Table 1).[23] Thus, our further discussion will be based on MP2/aVDZ++ values of PAs, unless otherwise specified.

We also carried out first principles CPMD simulations based on the BLYP functional for 10 ps at 150 K, using the CPMD code (version 3.9.2).[24] A fictitious electron mass of 600 a.u. and an integration step of $\Delta t = 4.135$ a.u (0.1 fs) were used in all of the simulations. A Nosé–Hoover thermostat[25] was attached to every degree of freedom to ensure proper thermalization over the CPMD trajectory. During the simulations, we kept the molecules at the center of an isolated cubic box of approximately twice the size of the longest internal coordinate. Poisson solver using the Tuckerman method on the reciprocal space was applied.[26] The core-valence interaction was described by a norm-conserving Troullier–Martins pseudopotential.[27] Valence wave functions were expanded in a plane wave basis set with an energy cutoff value of 90 Ry. Based on the CPMD simulations, we derived the time-correlation function to obtain the spectra of the clusters in the equilibrium state. The Fourier transformation of dipole-moment/velocity autocorrelation functions (FT-DACF/FT-VACF) was carried out.

The IR absorption spectrum can be computed from FT-DACF:

$$I(\omega) = \frac{\hbar\beta}{2\pi}\omega^2 \int \mathrm{d}t e^{-i\omega t}\langle\mu(0)\mu(t)\rangle.$$

Here, the symbols used denote intensity (I), frequency (ω), Planck's constant ($\hbar = h/2\pi$), inverse of Boltzmann's constant multiplied by temperature ($\beta = 1/kT$), time (t), and dipole moment (μ). For the computational purpose, it is more convenient to compute the autocorrelation function of the time derivative of the dipole moment:[28]

$$I(\omega) = \frac{\hbar\beta}{2\pi} \int \mathrm{d}t e^{-i\omega t}\langle\dot{\mu}(0)\dot{\mu}(t)\rangle.$$

Therefore, this method is employed in our calculations. Since FT-DACF provides the information about dipole moment change resulted from vibrational motions of molecule, FT-DACF is considered to be similar to the experimental IR spectrum. As another observable related to the IR spectra, FT-VACF is often used for the frequency analysis with intensities representing the rovibrational density of states.

Table 1 Proton affinities (PA) [kJ mol^{-1}] of monomers which constitute the H-bonded dimers[a]

Group	Monomer	Proton affinity/kJ mol^{-1}		μ/debye
		MP2/aVDZ++ (B3LYP/aVDZ++)	Expt.	MP2/aVDZ++ (B3LYP/aVDZ++)
Water	H_2O	697.1 (702.9)	690.8	2.02 (1.86)
Peroxide	H_2O_2	682.0 (687.8)	674.0	1.90 (1.75)
Alcohol	MeOH	773.6 (776.6)	754.0	1.83 (1.66)
Alcohol	EtOH	796.2 (802.9)	776.1	1.88 (1.71)
Aldehyde	HCHO	729.3 (737.6)	712.5	2.95 (2.41)
Aldehyde	MeCHO	783.7 (800.8)	768.2	3.36 (2.91)
Aldehyde	PhCHO	840.1 (869.4)	833.5	3.85 (3.53)
{Anhydride}[b]	$O(CHO)_2$	767.3 (772.8)	—	3.94 (3.31)
{Carboxyacid}[c]	HCOOH	685.3 (673.6)	—	1.74 (1.55)
Carboxyacid[d]	HCOOH	737.2 (749.8)	741.8	1.74 (1.55)
Methylperoxide	MeOOH	743.9 (747.3)	—	1.83 (1.66)
Ether	Me_2O	813.4 (806.3)	791.6	1.51 (1.27)
Ether	MeOEt	832.6 (838.5)	—	1.54 (1.32)
Ether	Et_2O	836.0 (850.6)	828.0	1.57 (1.34)
Ketone	Me_2CO	827.2 (848.1)	811.7	3.52 (3.11)
{Ketone}[e]	$(CN)_2CO$	623.4 (648.9)	—	0.49 (0.53)
Nitrile[f]	$(CN)_2CO$	676.1 (689.5)	—	0.49 (0.53)

[a] Braces in the column of "group" denote the PAs for non-natural systems because the nitrile group is better protonated than the carbonyl group, and the carbonyl group is better protonated than the ether group. [b] Anhydride protonated at the ether group. [c] Carboxyacid protonated at the OH group. [d] Carboxyacid protonated at the O=C group. [e] Ketone protonated at the O=C group. [f] Nitrile protonated at the N≡C group.

3. Results and discussion

The main goal of this manuscript is to analyze different –O···HO– motifs for various cationic (Fig. 1), anionic (Fig. 2), and neutral (Fig. 3) H-bonds in homogeneous and heterogeneous dimers.

We have performed geometry optimization and computed harmonic vibrational frequencies at the B3LYP and MP2 levels of theory. Fig. 1 shows the optimized structures at the MP2 level of theory. We scaled harmonic frequencies by employing the scaling factors (0.957 for MP2 and 0.963 for B3LYP) to obtain a reasonable agreement with the experimental data. We focused our attention on cationic dimers, because they usually form SSHBs. Moreover, to make our analysis complete, we have performed similar calculations for selected anionic and neutral forms. Because the anharmonicity is crucial for this class of compounds, we calculated IR

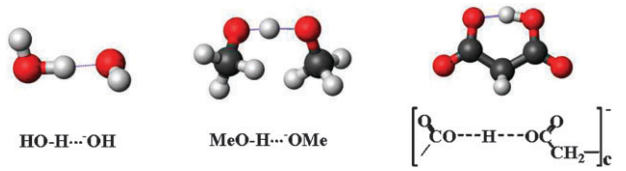

Fig. 2 MP2/aVDZ++ optimized structures for (anionic) deprotonated dimers.

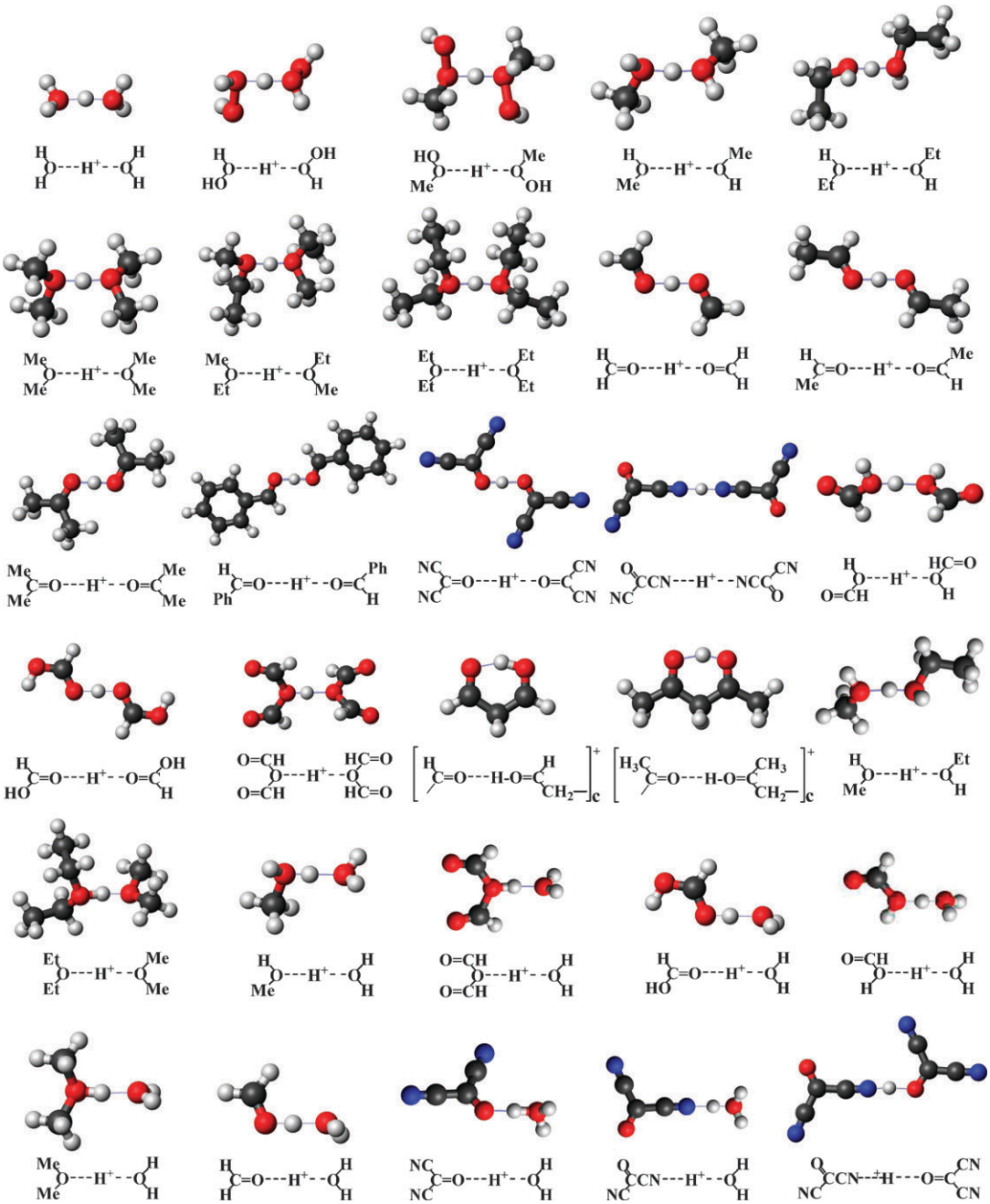

Fig. 1 MP2/aVDZ++ optimized structures for (cationic) protonated dimers.

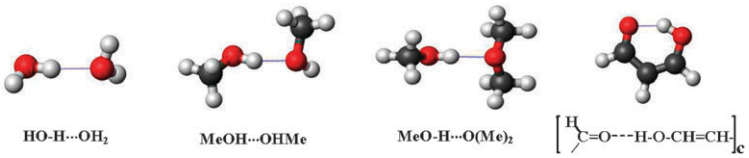

Fig. 3 MP2/aVDZ++ optimized structures for neutral H-bonded dimers.

absorption spectra for selected dimers derived from velocity- and dipole-autocorrelation functions obtained from CPMD simulations.

Table 2 lists the MP2/aVDZ++ (B3LYP/aVDZ++) geometrical parameters and binding energies (BEs) for the cationic dimers. The calculated interatomic distances at the B3LYP and MP2 levels of theory show almost the same trend. The SSHBs are formed for all cationic dimers. The inter-oxygen distances r(O1–O2) in the –O···H$^+$···O– motifs are around 2.4 Å for the homo-dimers, and they hardly exceed 2.5 Å even for hetero-dimers. In Table 2, for the hetero-dimers, we put the monomer with the larger PA on the left hand side. The r(O1–H) and r(O2–H) are the O–H bond distances on the left and right hand sides, respectively. The r(O1–H) bond lengths are shorter because the left monomer has larger PA. δr is defined as the difference between the two OH bond distances: $\delta r = r$(O2–H) − r(O1–H). In the natural homo-dimers (excluding the non-natural ones, which are presented in parentheses), δr is close to zero except for the intra-hydrogen-bonded systems whose δr is 0.2–0.3 Å (at the MP2 level of theory) because of slightly weakened SSHBs arising from the bent angle of the O–H–O motif (~155°). The shortest r(O···O) distance (2.40 Å) is found for the protonated homogeneous ethoxy-ethane dimer. The inter-nitrogen distance in the nitrilecarbonyl protonated homo-dimer (2.53 Å) is slightly longer, even though δr (0.006 Å) is almost zero, than the inter-oxygen distance in the protonated homo-dimers because the nitrogen atom has a slightly larger van der Waals radius than the oxygen atom.

Table 3 lists the frequencies corresponding to the symmetric and asymmetric stretching modes parallel to the O···O axis (denoted as ν_s) and the out-of-plane and in-plane bending vibrations roughly perpendicular to the same axis (denoted as ν_b) for the cationic dimers.[29] The dimers in parentheses in the column "group" in Tables 2 and 3 are non-natural systems (which require exquisite experiments to be done selectively with special techniques) because the nitrile group is more easily protonated than the carbonyl group, and the carbonyl group is more easily protonated than the ether group. For the O-containing vibrations of the protonated homo/hetero-dimers (by excluding the dimers in parentheses and nitriles in Table 3), the symmetric and asymmetric ν_s are 296–831 cm^{-1} and 649–2556 cm^{-1}, and the out-of-plane and in-plane ν_b are 1219–1551 cm^{-1} (ν_{bx}; out of plane) and 1230–1661 cm^{-1} (ν_{by}; in plane). It should be noted that two distinct O···H···O stretching modes exhibit only small splitting, however, the r(O1–H) and r(O2–H) distances are almost identical.

In Fig. 4, we examined the dependence of binding energies (BEs), H-bond distances r(O–O)/r(O1–H), and the vibrational frequencies (ν_s and ν_b) *versus* the difference between proton affinities of monomers (ΔPA) in the O-containing heterogeneous dimers [EtHO···H$^+$···OHMe, Et$_2$O···H$^+$···OMe$_2$, MeHO···H$^+$···OH$_2$, (OH)HCO···H$^+$···OH$_2$, Me$_2$O···H$^+$···OH$_2$, H$_2$C=O···H$^+$···OH$_2$]. While ΔPA decreases, the BE tends to increase, resulting in stronger H-bond. While the r(O–O) distance decreases, the symmetric ν_s and out-of-plane ν_{bx} tend to increase, but the asymmetric ν_s tends to decrease. Our theoretical results for the ΔPA *vs.* ν_s plot are in good agreement with the experimental data for a series of protonated dimers studied by Johnson and coworkers.[30]

The SSHBs are also formed in the case of anionic dimers. Anionic dimers have slightly longer r(O···O) distances (~2.5 Å) in comparison with cationic dimers, which results in less symmetric (less delocalized) H-bonds (δr = 0.2–0.3 Å) (Table 4) and slightly red-shifted symmetric and blue-shifted asymmetric ν_s frequencies (295–333 and 934–1516 cm^{-1}) (Table 5). The out-of-plane vibrations are slightly red-shifted and the in-plane vibrations ν_b are blue-shifted (1192–1329 and 1516–1599 cm^{-1}) (Table 5) in comparison with the cationic systems. It is important to note that the binding energy is closely related to the r(O···O) distance.

The neutral dimers do not form SSHBs, but the highly asymmetric (localized) H-bonds (δr = ~0.9 Å) are created. These inter-oxygen distances (~2.8 Å) are much longer than those of the cationic/anionic dimers (Table 6). The symmetric ν_s frequencies corresponding to O2–H vibrational modes range 176–269 cm^{-1}, the asymmetric ν_s frequencies corresponding to O1–H vibrational modes range 3007–3545 cm^{-1} (Table 7), and the out-of-plane and in-plane ν_b modes are 677–873 and 1343–1377 cm^{-1}. The 'intra-aldehyde–alcohol' structure has a short r(O···O) distance due to the sp-hybridization of oxygen and the delocalization of the O–H bond induced by the resonance effect through single–double bond conjugation. The asymmetric stretching mode is relatively red-shifted with respect to the typical neutral H-bonded systems.

We investigated the relationship between BEs and r(O1–O2) distances. The dimer with larger BE has smaller r(O–H2) distance. It shows that BE is roughly proportional to $[r(\text{O–H2})]^{-4}$, as shown in Fig. 5. This indicates that the H-bonding energy arises mainly from the polarization effect that a positively charged H atom (proton donor) polarizes the O atom (proton acceptor) in the neighboring molecule. This polarization energy is $-\frac{1}{2}\alpha e^2 Z_{\text{eff}}/r^4$, where α is the polarizability of the O atom (0.802 Å^3) and Z_{eff} is the effective charge of the H atom. If Z_{eff} = ~0.5 and r(O–H2) = ~1.5 or ~1.2 Å, the polarization energy gain is ~46 or ~117 kJ mol^{-1}, in reasonable agreement with the binding energy for each dimer. Thus, polarization plays the key role in diverse hydrogen bonding.

As for the O–H–O vibrational modes, in the cationic systems, the symmetric and asymmetric stretching modes ν_s (296–831 and 649–2556 cm^{-1}) are highly blue-shifted and

Table 2 MP2/aVDZ++ (B3LYP/aVDZ++) geometrical parameters (in Å or degree) and binding energies (BE in kJ mol^{-1}) for the (cationic) protonated dimers[a]

Group	Cationic dimer	BE	*r*(O1–O2)	*r*(O1–H)	*r*(O2–H)	δ*r*
	Homo-dimer					
Water	$H_2O\cdots H^+\cdots OH_2$	151.9 (154.0)	2.404 (2.404)	1.202 (1.202)	1.202 (1.202)	0.000 (0.000)
Peroxide	$H(OH)O\cdots H^+\cdots O(OH)H$	144.8 (138.5)	2.418 (2.424)	1.191 (1.195)	1.231 (1.230)	0.040 (0.035)
Peroxide	$Me(OH)O\cdots H^+\cdots O(OH)Me$	149.4 (132.2)	2.414 (2.416)	1.207 (1.209)	1.207 (1.209)	0.000 (0.000)
Alcohol	$MeHO\cdots H^+\cdots OHMe$	139.7 (137.7)	2.397 (2.400)	1.197 (1.190)	1.204 (1.212)	0.007 (0.022)
Alcohol	$EtHO\cdots H^+\cdots OHEt$	138.1 (132.2)	2.400 (2.402)	1.197 (1.173)	1.207 (1.232)	0.010 (0.059)
Ether	$Me_2O\cdots H^+\cdots OMe_2$	138.9 (135.6)	2.396 (2.396)	1.199 (1.200)	1.199 (1.200)	0.000 (0.000)
Ether	$EtMeO\cdots H^+\cdots OMeEt$	141.8 (121.8)	2.400 (2.404)	1.177 (1.137)	1.227 (1.269)	0.050 (0.132)
Ether	$Et_2O\cdots H^+\cdots OEt_2$	161.9 (127.2)	2.395 (2.400)	1.198 (1.150)	1.198 (1.253)	0.000 (0.103)
Aldehyde	$H_2C{=}O\cdots H^+\cdots O{=}CH_2$	135.6 (136.4)	2.421 (2.422)	1.210 (1.211)	1.210 (1.211)	0.000 (0.000)
Aldehyde	$MeHC{=}O\cdots H^+\cdots O{=}CHMe$	142.3 (141.4)	2.416 (2.416)	1.208 (1.208)	1.208 (1.208)	0.000 (0.000)
Ketone	$Me_2C{=}O\cdots H^+\cdots O{=}CMe_2$	140.6 (133.9)	2.421 (2.426)	1.173 (1.150)	1.248 (1.275)	0.075 (0.125)
Ketone	$PhHC{=}O\cdots H^+\cdots O{=}CHPh$	136.8 (135.6)	2.406 (2.417)	1.171 (1.141)	1.236 (1.276)	0.065 (0.135)
{Ketone}	$(CN)_2C{=}O\cdots H^+\cdots O{=}C(CN)_2$	81.6 (73.2)	2.448 (2.448)	1.134 (1.118)	1.314 (1.330)	0.180 (0.212)
Nitrile	$C{=}O(CN)CN\cdots H^+\cdots NC(CN)C{=}O$	103.3 (98.7)	2.528 (2.534)	1.261 (1.267)	1.267 (1.267)	0.006 (0.000)
{Carboxyacid}	$CHO(HO)\cdots H^+\cdots (OH)CHO$	65.7 (70.7)	2.462 (2.426)	1.081 (1.141)	1.382 (1.286)	0.301 (0.145)
Carboxyacid	$(HO)CHO\cdots H^+\cdots OCH(OH)$	145.2 (147.3)	2.409 (2.409)	1.204 (1.205)	1.204 (1.205)	0.000 (0.000)
{Anhydride}	$(OCH)_2O\cdots H^+\cdots O(CHO)_2$	107.1 (111.3)	2.463 (2.439)	1.069 (1.096)	1.399 (1.345)	0.330 (0.248)
Intra-ketone[b]	$[-HC{=}O\cdots H{-}O{=}CH{-}CH_2-]_c^+$	—	2.425 (2.435)	1.093 (1.076)	1.391 (1.433)	0.298 (0.357)
Intra-ketone[c]	$[-MeC{=}O\cdots H{-}O{=}CMe{-}CH_2-]_c^+$	—	2.400 (2.404)	1.117 (1.095)	1.330 (1.366)	0.213 (0.271)
	Hetero-dimer					
Alcohol {5}	$EtHO\cdots H^+\cdots OHMe$	129.7 (123.8)	2.421 (2.424)	1.110 (1.107)	1.314 (1.320)	0.204 (0.213)
Ether {5}	$Et_2O\cdots H^+\cdots OMe_2$	136.4 (113.4)	2.430 (2.452)	1.092 (1.067)	1.341 (1.388)	0.249 (0.321)
w–Alcohol {18}	$MeHO\cdots H^+\cdots OH_2$	117.6 (118.0)	2.473 (2.465)	1.055 (1.063)	1.424 (1.404)	0.369 (0.341)
{w–Anhydride} {17}	$(OCH)_2O\cdots H^+\cdots OH_2$	104.2 (106.3)	2.498 (2.486)	1.050 (1.060)	1.449 (1.426)	0.399 (0.367)
w–Carboxyacid {10}	$(OH)HCO\cdots H^+\cdots OH_2$	135.6 (134.3)	2.472 (2.468)	1.068 (1.074)	1.404 (1.394)	0.337 (0.321)
{w–Carboxyacid} {3}	$H_2O\cdots H^+\cdots (OH)CHO$	103.3 (98.7)	2.413 (2.414)	1.142 (1.163)	1.273 (1.252)	0.131 (0.089)
w–Ether {28}	$Me_2O\cdots H^+\cdots OH_2$	105.4 (112.5)	2.514 (2.509)	1.031 (1.033)	1.486 (1.477)	0.455 (0.444)
w–Aldehyde {8}	$H_2C{=}O\cdots H^+\cdots OH_2$	129.7 (129.3)	2.449 (2.447)	1.100 (1.108)	1.350 (1.340)	0.250 (0.232)
{w–Ketone} {18}	$H_2O\cdots H^+\cdots O{=}C(CN)_2$	83.3 (87.0)	2.488 (2.450)	1.071 (1.105)	1.418 (1.346)	0.347 (0.241)
w–Nitrile {5}	$H_2O\cdots H^+\cdots NC(CN)C{=}O$	119.2 (120.9)	2.509 (2.490)	1.094 (1.126)	1.416 (1.365)	0.322 (0.240)
{Nitrile–ketone} {13}	$(NC)(CO)CN\cdots H^+\cdots O{=}C(CN)_2$	121.8 (107.1)	2.522 (2.509)	1.138 (1.147)	1.386 (1.367)	0.248 (0.221)

[a] The dimers in braces in the column of "group" are non-natural less stable systems because the nitrile group is better protonated than the carbonyl group, and the carbonyl group is better protonated than the ether group. "w" denotes water. For the heterodimer, the values in braces denote ΔPA at the MP2/aVDZ++ level, where the monomer on the left side has the larger PA than that on the right side. The *r*(O1–H) and *r*(O2–H) are the O–H bond distances on the left and right sides, respectively. The *r*(O1–H) bond length is shorter because the left monomer has higher PA. δ*r* is the difference between two OH bond distances: δ*r* = *r*(O2–H) − *r*(O1–H). [b] The bending angle "*θ*" of (O–H–O) is 155°. [c] "*θ*" is 157°.

red-shifted due to the strong delocalization in the O1–H–O2 bonds, as compared with the ν_s of the typical neutral hydrogen bonding [176–269 cm^{-1} corresponding to O1–H vibrations and 3007–3545 cm^{-1} corresponding to O2–H vibrations]. The strong and weak O–H stretching modes in the neutral hydrogen bonds transform into the asymmetric and symmetric O–H–O stretching modes, respectively, in the cationic/anionic hydrogen bonds. In the anionic systems, the blue-shifted symmetric and red-shifted asymmetric stretching modes ν_s (295–333 and 934–1516 cm^{-1}) arise from partial delocalization of similar but non-identical O1–H and O2 –H bonds. The (out-of-plane and in-plane) ν_b are (1219–1551 and 1230–1661 cm^{-1}) for cationic dimers, (1192–1329 and 1516–1599 cm^{-1}) for the anionic systems, and (677–873 and 1343–1377 cm^{-1}) for the neutral systems.

The vibrational modes of hydrogen bonds have a broad IR spectrum due to the non-rigid (flexible) structure. The shared proton results in large amplitude motion even at its zero-point level. Since large-amplitude (~0.3 Å) motions are possible, the anharmonic effects should be considered. The scaled harmonic frequencies calculated at the MP2 and B3LYP levels of theory are far from the experimental data. In the case of ionic dimers, in particular, in the cationic homo-dimers, the anharmonicity is important to obtain realistic IR frequencies close to the experimental values. To take into account the anharmonicity, we carried out CPMD simulations, and obtained IR power spectra from dipole- and velocity-autocorrelation functions (Fig. 6). For cationic and anionic dimers, there is a broad spectrum between 850 and 2100 cm^{-1} as fingerprints of SSHBs.

The ν_s vibrational frequencies calculated from dipole- and velocity-autocorrelation functions taken from CPMD simulations are close to the experimental values (Table 8). However, in some cases they are slightly overestimated, as in the water-ether system. The anharmonic frequencies based on the minimal perturbation approach by using the Gaussian 03 suite of programs are worse than the corresponding CPMD results. Furthermore, the anharmonic frequency calculations are computationally very demanding, thus in practice such calculations are not feasible for large systems.

As we have confirmed theoretically, the PAs of monomers greatly affect the geometrical and spectral properties of dimers. Some test calculations for cationic dimers with different ΔPA are presented in Table 9. While ΔPA increases, the hydrogen bond becomes longer. The ΔPA greatly affects the IR spectrum of cationic dimers. As ΔPA increases, the BE

Table 3 MP2/aVDZ++ (B3LYP/aVDZ++) scaled harmonic frequencies (cm^{-1}) and their IR intensities (in subscripts in 10 km mol^{-1}) of O–H–O stretching and bending (ν_s and ν_b) for the (cationic) protonated dimers [scale factor: 0.963 (0.957)][a]

Group	Cationic dimer	ν_s	ν_b
	Homo-dimer		
Water	$H_2O\cdots H^+\cdots OH_2$	582_0, 779_{290} (579_0, 877_{270})	1401_{26}, 1463_{10} (1383_{24}, 1431_{10})
Peroxide	$H(OH)O\cdots H^+\cdots O(OH)H$	525_{19}, 985_{249} (498_{13}, 947_{208})	1551_{13}, 1570_{24} (1480_{16}, 1605_{24})
Peroxide	$Me(OH)O\cdots H^+\cdots O(OH)Me$	544_0, 993_{109} (533_0, 955_{60})	1410_4, 1661_{16} (1322_3, 1651_7)
Alcohol	$MeHO\cdots H^+\cdots OHMe$	531_{12}, 677_{277} (513_{14}, 697_{266})	1522_{14}, 1568_{31} (1496_{18}, 1546_{39})
Alcohol	$EtHO\cdots H^+\cdots OHEt$	575_0, 649_{270} (528_{53}, 675_{207})	1506_8, 1563_{33} (1477_{21}, 1546_{42})
Ether	$Me_2O\cdots H^+\cdots OMe_2$	521_0, 706_{300} (513_0, 684_{320})	1493_{27}, 1528_3 (1440_8, 1486_3)
Ether	$EtMeO\cdots H^+\cdots OMeEt$	509_{12}, 682_{196} (495_{13}, 726_{59})	1467_{37}, 1543_3 (1385_3, 1475_{15})
Ether	$Et_2O\cdots H^+\cdots OEt_2$	831_0, 987_{24} (761_5, 1010_{49})	1477_3, 1500_2 (1398_{14}, 1496_2)
Aldehyde	$H_2C{=}O\cdots H^+\cdots O{=}CH_2$	541_0, 712_{555} (525_{16}, 800_{512})	1398_8, 1586_{15} (1369_8, 1565_{21})
Aldehyde	$MeHC{=}O\cdots H^+\cdots O{=}CHMe$	653_0, 915_{87} (654_6, 913_{87})	1358_6, 1598_9 (1336_7, 1585_{13})
Ketone	$Me_2C{=}O\cdots H^+\cdots O{=}CMe_2$	702_{134}, 1050_{17} (596_{96}, 1063_{65})	1348_3, 1598_{15} (1311_5, 1580_{23})
Ketone	$PhHC{=}O\cdots H^+\cdots O{=}CHPh$	761_{414}, 956_{15} (655_{200}, 978_{197})	1341_4, 1615_2 (1317_5, 1612_{14})
{Ketone}	$(CN)_2C{=}O\cdots H^+\cdots O{=}C(CN)_2$	580_{63}, 1059_{581} (584_{41}, 1131_{510})	1267_6, 1528_{43} (1222_7, 1527_{100})
Nitrile	$C{=}O(CN)CN\cdots H^+\cdots NC(CN)C{=}O$	716_0, 1044_{10} (719_0, 1049_8)	1219_6, 1230_6 (1216_7, 1245_7)
{Carboxyacid}	$CHO(HO)\cdots H^+\cdots (OH)CHO$	208_{39}, 1890_{254} (199_{119}, 927_{13})	1093_{16}, 1527_8 (1429_{171}, 1507_{97})
Carboxyacid	$(HO)CHO\cdots H^+\cdots OCH(OH)$	728_{288}, 757_{199} (749_2, 771_{554})	1248_5, 1568_{17} (1250_5, 1552_{22})
{Anhydride}	$(OCH)_2O\cdots H^+\cdots O(CHO)_2$	645_{28}, 2149_{341} (662_{28}, 2244_{300})	1099_{20}, 1394_{10} (1082_{22}, 1412_{11})
Intra-ketone	$[-HC{=}O\cdots H{-}O{=}CH\text{-}CH_2\text{-}]_c^+$	329_{24}, 1901_{76} (327_{15}, 2055_{86})	1293_9, 1637_7 (1252_9, 1609_{15})
Intra-ketone	$[-MeC{=}O\cdots H{-}O{=}CMe\text{-}CH_2\text{-}]_c^+$	609_{29}, 1786_{43} (617_{19}, 1898_{74})	1293_7, 1649_{12} (1254_{13}, 1675_{11})
	Hetero-dimer		
Alcohol{5}	$EtHO\cdots H^+\cdots OHMe$	450_{33}, 1626_{194} (451_{27}, 1637_{297})	1454_{13}, 1525_{91} (1439_3, 1540_{39})
Ether{5}	$Et_2O\cdots H^+\cdots OMe_2$	479_{14}, 1723_{343} (472_9, 1995_{353})	1369_4, 1534_2 (1250_{13}, 1498_3)
w–Alcohol {18}	$MeHO\cdots H^+\cdots OH_2$	369_9, 2208_{289} (373_9, 2130_{299})	1310_7, 1632_3 (1284_{10},1609_3)
{w–Anhydride} {17}	$(OCH)_2O\cdots H^+\cdots OH_2$	261_{11}, 2236_{313} (272_{11}, 2111_{276})	1132_{10}, 1387_{12} (1167_{10}, 1414_{12})
w–Carboxyacid{10}	$(OH)HCO\cdots H^+\cdots OH_2$	323_{12}, 2046_{339} (325_{14}, 2001_{321})	1275_6, 1310_7 (1264_8, 1305_7)
{w–Carboxyacid} {3}	$H_2O\cdots H^+\cdots (OH)CHO$	738_{89}, 974_{53} (711_{94}, 951_{46})	1409_{71}, 1513_6 (1412_{58}, 1467_7)
w–Ether {28}	$Me_2O\cdots H^+\cdots OH_2$	296_3, 2556_{245} (288_3, 2522_{252})	1247_6, 1490_4 (1122_3, 1497_3)
w–Aldehyde {8}	$H_2C{=}O\cdots H^+\cdots OH_2$	445_{23}, 1735_{274} (431_{21}, 1720_{233})	1419_{13}, 1462_8 (1350_{87}, 1445_8)
{w–Ketone} {18}	$H_2O\cdots H^+\cdots O{=}C(CN)_2$	319_{19}, 1988_{333} (354_{25}, 1344_{267})	1108_{12}, 1629_5 (1119_{11}, 1586_6)
w–Nitrile {5}	$H_2O\cdots H^+\cdots NC(CN)C{=}O$	291_{12}, 1752_{317} (322_{17}, 1239_{286})	1112_{19}, 1600_1 (1102_{17}, 1558_5)
{Nitrile–ketone} {13}	$(NC)(CO)CN\cdots H^+\cdots O{=}C(CN)_2$	566_{17}, 1393_{586} (500_{17}, 1314_{665})	1176_6, 1214_{41} (1185_7, 1211_{97})

[a] See the footnote of Table 2.

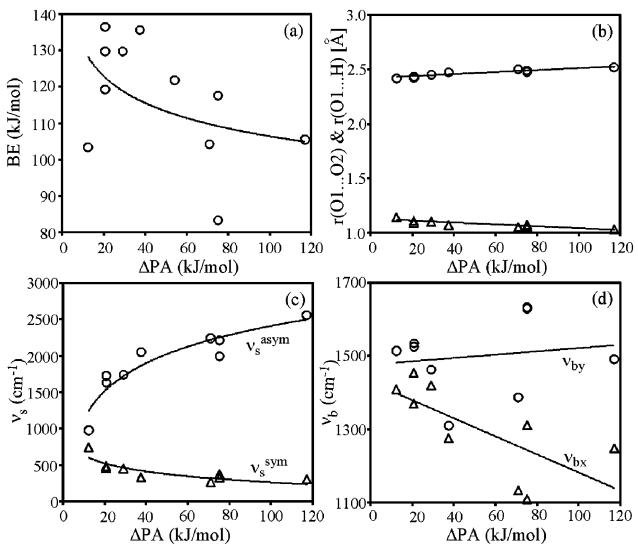

Fig. 4 Dependence of the binding energies (BE in kJ mol^{-1}) (a) and the r(O1···O2) and r(O1···H) distances (in Å) (b) on the difference in proton affinities (ΔPA in kJ mol^{-1}) for the (cationic) protonated heterodimers in Tables 2 and 3, and the same plots for ν_s (c) and ν_b (d) (in cm^{-1}) for the nine heterodimers.The MP2/aVDZ++ data were used. The w–nitrile and nitrile–ketone are excluded. There are two stretching modes (asymmetric ν_s^{asym} and symmetric ν_s^{sym}) and two bending modes (out-of-plane ν_{bx} and in-plane ν_{by}) in the O–H–O motif.

tends to decrease (though poorly), the asymmetric stretching vibrational mode ν_s is blue-shifted, and the corresponding out-of-plane bending modes ν_b are red-shifted. This procedure is applicable only to heterogeneous dimers. If the difference in proton affinities is substantially large, the SSHB is not formed. However, such a simple criterion in terms of ΔPA is useful for the design of novel molecular systems with SSHBs in the field of supramolecular chemistry.

4. Conclusions

We have carried out DFT and MP2 calculations for various cationic, anionic, and neutral dimers. We performed geometry optimization and computed harmonic vibrational frequencies. The main goal of our research was to investigate the dimers with SSHB in –O···H···O– motifs. The SSHB is specified by geometric parameters as well as characteristic vibrational modes in the IR spectrum. For all the cationic dimers, the SSHB was formed. The calculated harmonic frequencies are within the range typical for SSHBs. For anionic dimers, the SSHB is formed in all cases. In ionic systems, the O–H–O asymmetric stretching vibrational frequencies are red-shifted and the symmetric stretching vibrational frequencies are blue-shifted in comparison with the neutral dimers. In the case of neutral dimers, the SSHB is not formed. Since the anharmonicity is crucial for these ionic hydrogen bonds, we carried out

Table 4 MP2/aVDZ++ (B3LYP/aVDZ++) geometrical parameters (in Å or degree) and binding energies (BE in kJ mol^{-1}) for the (anionic) deprotonated dimers

Group	Anionic dimer	BE	r(O1–O2)	r(O1–H)	r(O2–H)	δr
Water	$(HO\cdots H\cdots OH)^-$	110.5 (113.0)	2.512 (2.491)	1.092 (1.111)	1.420 (1.381)	0.328 (0.270)
Alcohol	$(MeO\cdots H\cdots OMe)^-$	118.0 (108.4)	2.445 (2.460)	1.126 (1.103)	1.321 (1.357)	0.195 (0.254)
Intra-carboxyacid[a]	$[–OCO\cdots H\cdots OCO\text{-}CH_2–]_c^-$	—	2.437 (2.433)	1.090 (1.087)	1.370 (1.375)	0.280 (0.288)

[a] "θ" is 164°.

Table 5 MP2/aVDZ++ (B3LYP/aVDZ++) scaled harmonic frequencies (cm^{-1}) and their IR intensities (in subscripts in 10 km mol^{-1}) of O–H–O stretching and bending (ν_s and ν_b) for the (anionic) deprotonated dimers

Group	Anionic dimer	ν_s	ν_b
Water	$(HO\cdots H\cdots OH)^-$	309_{26}, 1516_{243} (309_{37}, 1340_{259})	1267_6, 1516_{243} (559_1, 1285_{80})
Alcohol	$(MeO\cdots H\cdots OMe)^-$	333_{94}, 934_{210} (346_{57}, 1536_{101})	1329_3, 1562_{10} (1308_{20}, 1516_{89})
Intra-carboxyacid	$[–OCO\cdots H\cdots OCO–CH_2–]_c^-$	295_{19}, 1465_{181} (298_{16}, 1484_{179})	1192_5, 1599_{46} (1199_5, 1618_{50})

Table 6 MP2/aVDZ++ (B3LYP/aVDZ++) geometrical parameters (in Å or degree) and binding energies (BE in kJ mol^{-1}) for the neutral H-bonded dimers

Group	Neutral dimer	BE	r(O1–O2)	r(O1–H)	R(O2–H)	δr
Water	$HO–H\cdots OH_2$	22.2 (19.7)	2.920 (2.910)	0.973 (0.973)	1.951 (1.945)	0.978 (0.972)
Alcohol	$MeO–H\cdots OHMe$	26.8 (20.9)	2.846 (2.883)	0.974 (0.972)	1.886 (1.915)	0.912 (0.943)
Alcohol–ether	$MeO–H\cdots OMe_2$	30.1 (20.9)	2.807 (2.868)	0.975 (0.973)	1.857 (1.900)	0.882 (0.927)
Intra-aldehyde–alcohol[a]	$[–HC{=}O\cdots H–O–CH{=}CH–]_c$	—	2.583 (2.570)	1.002 (1.004)	1.673 (1.666)	0.671 (0.662)

[a] "θ" is 160°.

Table 7 MP2/aVDZ++ (B3LYP/aVDZ++) scaled harmonic frequencies (cm^{-1}) and their IR intensities (in subscripts in 10 km mol^{-1}) of O–H–O stretching and bending (ν_s and ν_b) for neutral H-bonded dimers

Group	Neutral dimer	ν_s	ν_b
Water	$HO–H\cdots OH_2$	178_{15}, 3545_{28} (177_{16}, 3535_{34})	342_6, 610_9 (350_5, 613_9)
Alcohol	$MeO–H\cdots OHMe$	184_1, 3516_{49} (171_1, 3524_{53})	677_{10}, 1374_3 (654_7, 1365_4)
Alcohol–ether	$MeO–H\cdots OMe_2$	176_1, 3480_{56} (155_1, 3511_{59})	689_6, 1377_6 (658_6, 1366_4)
Intra-aldehyde–alcohol	$[–HC{=}O\cdots H–O–CH{=}CH–]_c$	269_1, 3007_{19} (272_1, 2966_{24})	873_3, 1343_5 (910_4, 1349_5)

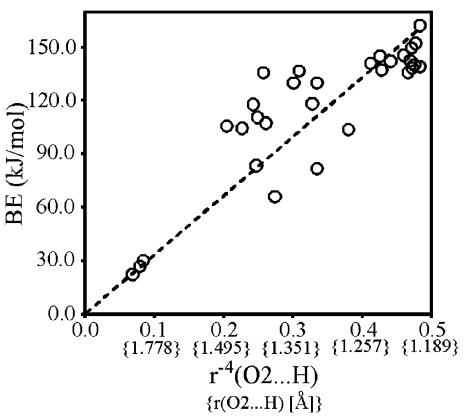

Fig. 5 The relationship between BEs and the r(O2···H) for all conformers in cation, anion and neural H-bond systems at the MP2/aVDZ++ level of theory.

CPMD simulations, and calculated the IR spectrum from the velocity- and dipole-autocorrelation functions. The IR spectra derived from CPMD simulations confirm that all the cationic/anionic dimers form SSHB. There are interesting relationships between ΔPA and various geometrical and spectral features of cationic dimers. For larger ΔPA, the asymmetric and symmetric stretching vibrational modes ν_s are blue-shifted and red-shifted, respectively, and the in-plane ν_{by} vibrational modes are blue-shifted. This is consistent with Johnson's experimental results.[30]

As for the O–H–O vibrational modes, in the cationic dimers, the ν_s (296–831 and 649–2556 cm^{-1}) corresponding to the symmetric and asymmetric stretching modes are more highly blue-shifted and more highly red-shifted due to the strong delocalization of nearly symmetric r(O1–H) and r(O2–H) bonds than the ν_s of the typical neutral hydrogen bonds [176–269 cm^{-1} corresponding to r(O1–H) and 3007–3545 cm^{-1} corresponding to r(O2–H)], respectively. In the anionic systems, the ν_s (295–333 and 934–1516 cm^{-1}) corresponding to the symmetric and asymmetric stretching modes stem from the partial delocalization of similar but non-equivalent r(O1–H) and r(O2–H) bonds. In the systems with strong H-bond interactions (large binding energies), the weak O···H bond becomes stronger and the strong O–H bond becomes weaker, and the weak O···H stretching mode (symmetric O–H–O stretching mode) is blue-shifted and the strong O–H stretching mode (asymmetric O–H–O stretching mode) is red-shifted. The cationic/anionic H-bond systems

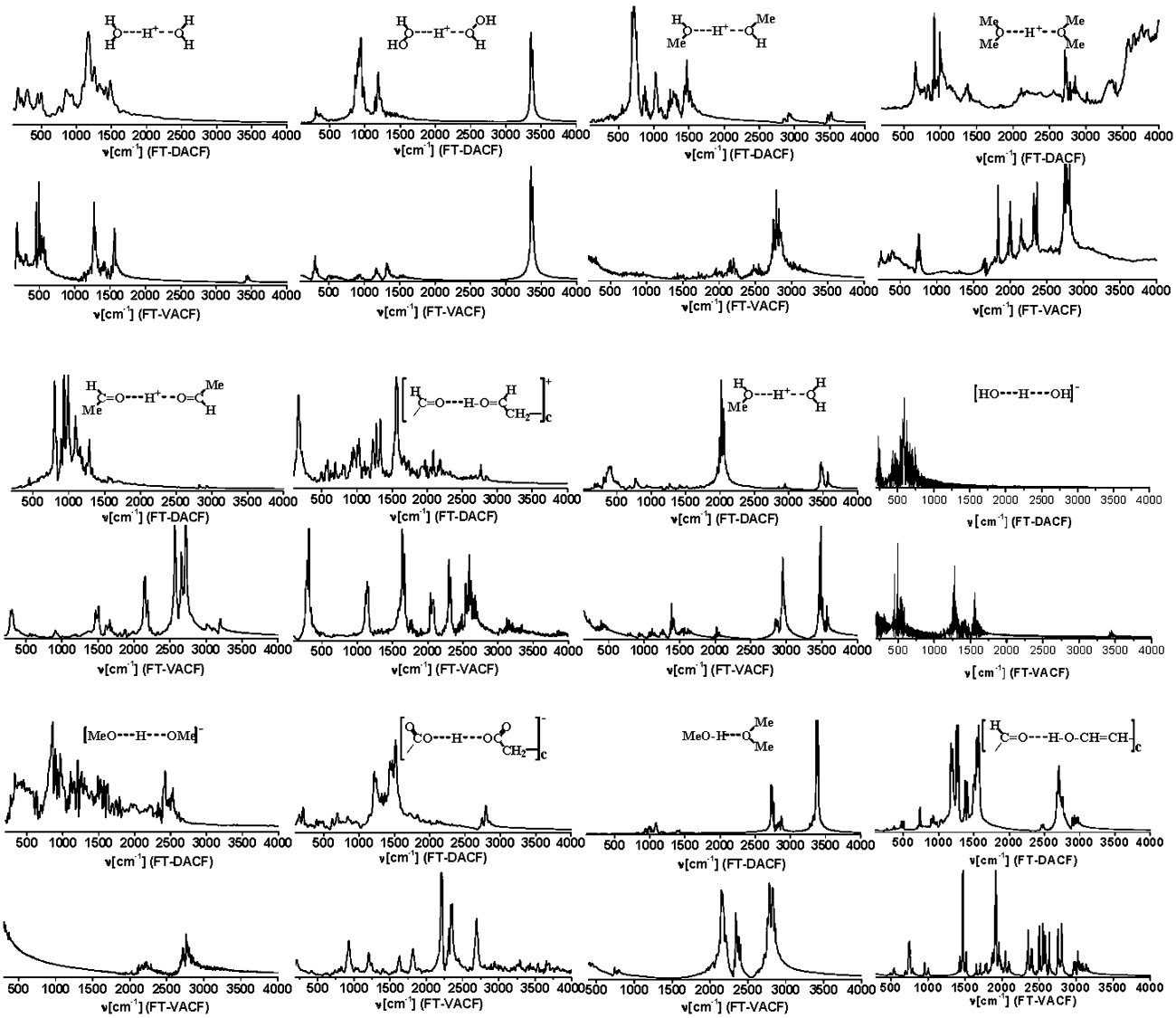

Fig. 6 CPMD power IR spectra derived from dipole- and velocity-autocorrelation function (DVCF and VACF) for the selected cationic, anionic and neutral dimers.

Table 8 MP2/aVDZ++ scaled harmonic (scaled factor: 0.957) and unscaled anharmonic frequencies and CPMD(BLYP) frequencies for the OHO ν_s vibrational mode of the (cationic) protonated dimers (frequencies in cm^{-1})

Group	Cation dimer	Harmonic	Anharmonic	CPMD	Expt.[a]
Water	$H_2O\cdots H^+\cdots OH_2$	779	1064	980	1002
Alcohol	$MeHO\cdots H^+\cdots OHMe$	677	800	878	887
Ether	$Me_2O\cdots H^+\cdots OMe_2$	878	—[b]	920	952
w-Alcohol	$H_2O\cdots H^+\cdots OHMe$	2208	1601	2020	1828
w-Ether	$H_2O\cdots H^+\cdots OMe_2$	2556	2385	2427	2094

[a] The experimental frequencies are from ref. 30. [b] This calculation was not possible because it was computationally very demanding.

have a relatively large binding energy in comparison with the neutral forms. Therefore, the asymmetric stretching mode is red-shifted and the symmetric stretching mode is blue-shifted as compared with neutral systems of weak H-bond interactions.

The systems comprising SSHBs are characterized by broad and complex IR spectra. The harmonic vibrational analysis seems to be insufficient to properly interpret the experimental results. The anharmonic frequencies based on the minimal perturbation approach are slightly improved, but still far from the experimental vibrational frequencies. The useful method is based on the Fourier transform of velocity- and dipole-autocorrelation function taken from CPMD simulations. While this approach is computationally very demanding, it gives reliable vibrational frequencies, close to the experimental values.

Table 9 MP2/aVDZ++ geometrical parameters (in Å or degree), binding energies (kJ mol^{-1}), and scaled H-bonded OH stretching frequencies ν_s (in cm^{-1}; scale factor: 0.957) for the (cationic) protonated dimers having the difference in proton affinities ΔPA (kJ mol^{-1}) between the monomers comprising the dimer[a]

Group	Cationic dimer	BE	ΔPA	r(O–O/Ar)	r(O/Ar···H)	ν_s
Acid–ester	Me(HO)C=O···H^+···O=CHOMe	120.5	0 [0]	2.46	1.08	1901
Alcohol–aldehyde	MeHO···H^+···O=CH_2	119.2	44.4 [41.4]	2.47	1.08	1912
CO_2–alcohol	OC=O···H^+···OHMe	54.0	222.2 [213.8]	2.63	1.00	3099
CO–alcohol	CO···H^+···OHMe	28.5	350.6 [328.0]	2.76	0.99	3292
Aldehyde–Ar	H_2C=O···H^+···Ar	18.4	353.1 [343.5]	3.15	1.00	3232

[a] The experimental values of ΔPA from ref. 24 are given in brackets along with the calculated values.

Through analysis of cationic, anionic and neutral homogeneous and heterogeneous dimers, these systems are investigated in terms of geometrical parameters of –O···H···O– motif, binding energies, and harmonic and anharmonic vibrational frequencies. The hydrogen bond energy is found to be roughly proportional to $[r(O/N–H)]^{-4}$. Thus, the polarization of the proton accepting O/N atom by the proton-donating H atom plays a key role in these hydrogen bonds, and such polarization energy reflects most of the binding energy in diverse cation/anion/neutral hydrogen bonds. The present study gives a deep insight into the nature of hydrogen-bonded dimers with SSHBs.

Acknowledgements

This work was supported by NRF (WCU: R32-2008-000-10180-0, EPB Center: 2009-0063312, BK21, GRL) and KISTI (KSC-2008-K08-0002).

Notes and references

1 (*a*) S. Scheiner, *Hydrogen Bonding: A Theoretical Perspective*, Oxford, New York, 1997; (*b*) *Hydrogen Bonding—New Insights*, ed. S. J. Grabowski, Springer, Dortrecht, Netherlands, 2006; (*c*) C. Pak, H. M. Lee, J. C. Kim, D. Kim and K. S. Kim, *Struct. Chem.*, 2005, **16**, 187–202.

2 (*a*) U. Buck and F. Huisken, *Chem. Rev.*, 2000, **100**, 3863–3890; (*b*) H. M. Lee, S. B. Suh, J. Y. Lee, P. Tarakeshwar and K. S. Kim, *J. Chem. Phys.*, 2000, **112**, 9759–9772.

3 (*a*) *Ion Solvation*, ed. Y. Marcus, Wiley, New York, 1985; (*b*) N. J. Singh, A. C. Olleta, A. Kumar, M. Park, H.-B. Yi, I. Bandyopadhyay, H. M. Lee, P. Tarakeshwar and K. S. Kim, *Theor. Chem. Acc.*, 2006, **115**, 127–135.

4 (*a*) S. Re, Y. Osamura, Y. Suzuki and H. F. Schaefer III, *J. Chem. Phys.*, 1998, **109**, 973–977; (*b*) S. Odde, B. J. Mhin, S. Lee, H. M. Lee and K. S. Kim, *J. Chem. Phys.*, 2004, **120**, 9524–9535; (*c*) A. Kumar, M. Park, J. Y. Huh, H. M. Lee and K. S. Kim, *J. Phys. Chem. A*, 2006, **110**, 12484–12493.

5 G. A. Jeffrey and W. Saenger, *Hydrogen Bonding in Biological Structures*, Springer-Verlag, 1991.

6 (*a*) J. M. Lehn, *Supramolecular Chemistry: Concepts and Perspectives*, VCH, Weinheim, 1995; (*b*) N. J. Singh, H. M. Lee, I.-C. Hwang and K. S. Kim, *Supramol. Chem.*, 2007, **19**, 321–332.

7 B. H. Hong, J. Y. Lee, C.-W. Lee, J. C. Kim, S. C. Bae and K. S. Kim, *J. Am. Chem. Soc.*, 2001, **123**, 10748–10749.

8 (*a*) J. Yoon, S. K. Kim, N. J. Singh and K. S. Kim, *Chem. Soc. Rev.*, 2006, **35**, 355–360; (*b*) H. Ihm, S. Yun, H. G. Kim, J. K. Kim and K. S. Kim, *Org. Lett.*, 2002, **4**, 2897–2900.

9 (*a*) W. W. Cleland and M. M. Kreevoy, *Science*, 1994, **264**, 1887–1890; (*b*) P. A. Frey, S. A. Whitt and J. B. Tobin, *Science*, 1994, **264**, 1927–1930; (*c*) Z. R. Wu, S. Ebrahimian, M. E. Zawrotny, L. D. Thornburg, G. C. Perez-Alvarado, P. Brothers, R. M. Pollack and M. F. Summers, *Science*, 1997, **276**, 415–418; (*d*) K. S. Kim, K. S. Oh and J. Y. Lee, *Proc. Natl. Acad. Sci. U. S. A.*, 2000, **97**, 6373–6378; (*e*) C. L. Perrin and J. B. Nielson, *Annu. Rev. Phys. Chem.*, 1997, **48**, 511.

10 N. Agmon, *Chem. Phys. Lett.*, 1995, **244**, 456.

11 (*a*) A. K. Soper, F. Bruni and M. A. Ricci, *J. Chem. Phys.*, 1997, **106**, 247–254; (*b*) S. W. Peterson and H. A. Levy, *Acta Crystallogr.*, 1957, **10**, 70–76.

12 S. B. Suh, J. C. Kim, Y. C. Choi, S. Yun and K. S. Kim, *J. Am. Chem. Soc.*, 2004, **126**, 2186–2193.

13 M. Ardon, A. Bino and W. G. Jackson, *Polyhedron*, 1987, **6**, 181.

14 (*a*) P. Vishweshwar, N. J. Babu, A. Nangia, S. A. Mason, H. Puschmann, R. Mondal and J. A. K. Howard, *J. Phys. Chem. A*, 2004, **108**, 9406–9416; (*b*) V. Bertolasi, P. Gilli, V. Ferretti and G. Gilli, *Chem.–Eur. J.*, 1996, **2**, 925.

15 (*a*) Y. Xie, R. B. Remington and H. F. Schaefer III, *J. Chem. Phys.*, 1994, **101**, 4878–4884; (*b*) D. Wei and D. R. Salahub, *J. Chem. Phys.*, 1994, **101**, 7633–7642; (*c*) H. M. Lee, P. Tarakeshwar, J. Park, M. R. Kolaski, Y. J. Yoon, H.-B. Yi, W. Y. Kim and K. S. Kim, *J. Phys. Chem. A*, 2004, **108**, 2949–2958; (*d*) E. F. Valeev and H. F. Schaefer III, *J. Chem. Phys.*, 1998, **108**, 7197–7201; (*e*) X. Huang, B. J. Braams and J. M. Bowman, *J. Chem. Phys.*, 2005, **122**, 044308; (*f*) M. Kaledin, A. L. Kaledin and J. M. Bowman, *J. Phys. Chem. A*, 2006, **110**, 2933; (*g*) M. Park, I. Shin, N. J. Singh and K. S. Kim, *J. Phys. Chem. A*, 2007, **111**, 10692–10702.

16 (*a*) G. K. H. Madsen, C. Wilson, T. M. Nymand, G. J. McIntyre and F. K. Larsen, *J. Phys. Chem. A*, 1999, **103**, 8684–8690; (*b*) J. Sørensen, H. F. Clausen, R. D. Poulsen, J. Overgaard and B. Schiott, *J. Phys. Chem. A*, 2007, **111**, 345–351; (*c*) M. C. Etter, Z. Urbanczyk-Lipkowska, D. A. Jahn and J. Frye, *J. Am. Chem. Soc.*, 1986, **108**, 5871–5876; (*d*) B. Hsu and E. O. Schlemper, *Acta Crystallogr., Sect. B: Struct. Crystallogr. Cryst. Chem.*, 1980, **36**, 3017; (*e*) F. Takusagawa and T. F. Koetzle, *Acta Crystallogr., Sect. B: Struct. Crystallogr. Cryst. Chem.*, 1978, **34**, 1149; (*f*) E. O. Schlemper, W. C. Hamiltom and S. J. La Placa, *J. Chem. Phys.*, 1971, **54**, 3990–4000; (*g*) H. van Koningsveld and F. R. Vevema, *Acta Crystallogr., Sect. C: Cryst. Struct. Commun.*, 1991, **47**, 289; (*h*) W. Joswig, H. Fuess and G. Ferraris, *Acta Crystallogr., Sect. B: Struct. Crystallogr. Cryst. Chem.*, 1982, **38**, 2798; (*i*) L. W. Schroeder and E. Prince, *Acta Crystallogr., Sect. B: Struct. Crystallogr. Cryst. Chem.*, 1976, **32**, 3309; (*j*) B. R. James, R. H. Morris, F. W. B. Einsten and A. Willis, *J. Chem. Soc., Chem. Commun.*, 1980, 31; (*k*) M. S. Hussain and E. O. Schlemper, *J. Chem. Soc., Dalton Trans.*, 1982, 751; (*l*) M. S. Hussain and E. O. Schlemper, *J. Chem. Soc., Dalton Trans.*, 1980, 750; (*m*) F. A. Cotton, C. K. Fair, G. E. Lewis, G. N. Mott, F. K. Ross, A. J. Schultz and J. M. Williams, *J. Am. Chem. Soc.*, 1984, **106**, 5319–5323.

17 J. C. MacDonald, P. C. Dorrestein and M. M. Pilley, *Cryst. Growth Des.*, 2001, **1**, 29.

18 (*a*) B. Chan, J. E. Del Bene and L. Radom, *J. Am. Chem. Soc.*, 2007, **129**, 12197–12199; (*b*) M. B. Burt and T. D. Fridgen, *J. Phys. Chem. A*, 2007, **111**, 10738.

19 F. Fontaine-Vive, M. R. Johnson, G. J. Kearley, J. A. K. Howard and S. F. Parker, *J. Am. Chem. Soc.*, 2006, **128**, 2963–2969.

20 I. Shin, M. Park, S. K. Min, E. C. Lee, S. B. Suh and K. S. Kim, *J. Chem. Phys.*, 2006, **125**, 234305.

21 (*a*) J. M. Headrick, E. G. Diken, R. S. Walters, N. I. Hammer, R. A. Christie, J. Cui, E. M. Myshakin, M. A. Duncan, M. A. Johnson and K. D. Jordan, *Science*, 2005, **308**, 1765–1769; (*b*) M. Miyazaki, A. Fujii, T. Ebata and N. Mikami,

Science, 2004, **304**, 1134–1137; (*c*) J.-W. Shin, N. I. Hammer, E. G. Diken, M. A. Johnson, R. S. Walters, T. D. Jaeger, M. A. Duncan, R. A. Christie and K. D. Jordan, *Science*, 2004, **304**, 1137–1140; (*d*) N. J. Singh, M. Park, S. K. Min, S. B. Suh and K. S. Kim, *Angew. Chem., Int. Ed.*, 2006, **45**, 3795–3800; (*e*) G. Niedner-Schatteburg, *Angew. Chem., Int. Ed.*, 2008, **47**, 1008–1011; (*f*) B. J. Bythell, U. Erlekam, B. Paizs and P. Maître, *ChemPhysChem*, 2009, **10**, 883.

22 M. J. Frisch, G. W. Trucks, H. B. Schlegel, G. E. Scuseria, M. A. Robb, J. R. Cheeseman, J. A. Montgomery, Jr., T. Vreven, K. N. Kudin, J. C. Burant, J. M. Millam, S. S. Iyengar, J. Tomasi, V. Barone, B. Mennucci, M. Cossi, G. Scalmani, N. Rega, G. A. Petersson, H. Nakatsuji, M. Hada, M. Ehara, K. Toyota, R. Fukuda, J. Hasegawa, M. Ishida, T. Nakajima, Y. Honda, O. Kitao, H. Nakai, M. Klene, X. Li, J. E. Knox, H. P. Hratchian, J. B. Cross, C. Adamo, J. Jaramillo, R. Gomperts, R. E. Stratmann, O. Yazyev, A. J. Austin, R. Cammi, C. Pomelli, J. W. Ochterski, P. Y. Ayala, K. Morokuma, G. A. Voth, P. Salvador, J. J. Dannenberg, V. G. Zakrzewski, S. Dapprich, A. D. Daniels, M. C. Strain, O. Fartas, D. K. Malick, A. D. Rabuck, K. Raghavachari, J. B. Foresman, J. V. Ortiz, Q. Cui, A. G. Baboul, S. Clifford, J. Cioslowski, B. B. Stefanov, G. Liu, A. Liashenko, P. Piskorz, I. Komaromi, R. L. Martin, D. J. Fox, T. Keith, M. A. Al-Laham, C. Y. Peng, A. Nanayakkara, M. Challacombe, P. M. W. Gill, B. Johnson, W. Chen, M. W. Wong, C. Gonzalez and J. A. Pople, *GAUSSIAN 03 (Revision B.1)*, Gaussian Inc., Wallingford, CT, 2004.

23 Proton Affinity Evaluation, E. P. Hunter and S. G. Lias, in *NIST Chemistry WebBook NIST Standard Reference Database Number 69*, ed. P. J. Linstrom and W. G. Mallard, National Institute of Standards and Technology, Gaithersburg MD, March 2003 (http://webbook.nist.gov).

24 J. Hütter, A. Alavi, T. Deutsch, M. Bernasconi, S. Goedecker, D. Marx, M. E. Tuckermann and M. Parrinello, CPMD, Version 3.9.2, Copyright IBM Corp. 1990–2005, Copyright MPI für Festkörperforschung, Stuttgart, 1997–2001.

25 (*a*) S. J. Nosé, *J. Chem. Phys.*, 1984, **81**, 511–519; (*b*) S. Nosé, *Mol. Phys.*, 1984, **52**, 255; (*c*) W. G. Hoover, *Phys. Rev. A: At., Mol., Opt. Phys.*, 1985, **31**, 1695.

26 G. J. Martyna and M. E. Tuckerman, *J. Chem. Phys.*, 1999, **110**, 2810–2821.

27 (*a*) N. Troullier and J. L. Martins, *Phys. Rev. B: Condens. Matter*, 1991, **43**, 1993–2006; (*b*) M. Sprik, J. Hutter and M. J. Parrinello, *J. Chem. Phys.*, 1996, **105**, 1142.

28 U. W. Schmitt and G. A. Voth, *J. Chem. Phys.*, 1999, **111**, 9361–9381.

29 E. G. Diken, J. M. Headrick, J. R. Roscioli, J. C. Bopp and M. A. Johnson, *J. Phys. Chem. A*, 2005, **109**, 1487–1490.

30 J. R. Roscioli, L. R. McCunn and M. A. Johnson, *Science*, 2007, **316**, 249–254.